Available online at www.sciencedirect.com
ScienceDirect
Precision Engineering 32 (2008) 126–133
PRECISION ENGINEERING
www.elsevier.com/locate/precision

Case study: A comparison of error sources in high-speed milling

Tony L. Schmitz [a,*], John C. Ziegert [b], J. Suzanne Canning [c], Raul Zapata [a]

[a] *University of Florida, Gainesville, FL, United States*
[b] *Clemson University, Clemson, SC, United States*
[c] *BWXT Y-12, Oak Ridge, TN, United States*

Received 6 April 2007; received in revised form 16 May 2007; accepted 15 June 2007
Available online 28 June 2007

Abstract

This paper describes a case study devised to quantify the relative contributions of geometric, thermal, contouring, and cutting force errors to machined part dimensional errors. Measurements were performed to independently evaluate the: (1) quasi-static geometric errors using the laser ball bar; (2) variations in geometric errors due to thermal effects; (3) spindle thermal growth errors using a capacitance gage nest; (4) two-dimensional contouring errors using a grid plate encoder; and (5) surface location error due to (stable) forced vibrations during cutting. The effects of the first three error components were related to part dimensions using a homogeneous transformation matrix approach integrated into a Monte Carlo simulation. A comparison of the individual influences of these error sources showed that the cutting force error was dominant for the high-speed machining center/tool-holder combination selected for this study.

Keywords: Machine tool; Accuracy; Geometric; Thermal; Controller; Dynamics; Force

1. Introduction

The accuracy of parts produced by machining operations has been studied extensively over the past 80 years or more (see early work by Schlesinger and Koenigsberger [1] and overview in [2]). It is known that machined part accuracy, or "the degree of conformance of the finished part to dimensional and geometric specifications" [2], has four major contributors: geometric errors of the machine construction, thermally induced errors from heat sources associated with the machine/cutting process, trajectory following errors caused by controller and machine structural dynamics, and errors due to the cutting forces. In computer numerically controlled (CNC) milling, the desired spatial trajectory of the rotating cutter is defined by the part program. The purpose of the part program is to place the tool tip at particular coordinates relative to the part at every instant in time, leaving behind newly created surfaces which form a workpiece of the proper dimensions. Errors in the final dimensions of the machined part are determined by the accuracy with which the commanded tool trajectory is followed, combined with any deflections of the tool, part/fixture, or machine caused by the cutting forces.

As part accuracy demands have increased, these error sources have received significant attention from researchers and machine tool builders alike. Due to these efforts, manufacturers now implement sophisticated error compensation algorithms to reduce the effect of geometric errors in the machine structure. Improved designs combined with software error compensation have reduced the effect of thermal error, although this can still be a major contributor. High performance axis drives coupled with modern control algorithms have improved trajectory following dramatically. Pre- or in-process compensation for milling force errors is less common, however.

In this paper, a case study performed on a new high-speed machining center (Mikron UCP-600 Vario[1]) is described where the contributions of the geometric, thermal, controller, and cutting force errors to inaccuracies in geometry for the well-known circle–diamond–square test part [3] have been quantified. The paper is organized as follows. First, tests to identify the

* Corresponding author. Tel.: +1 352 392 8909; fax: +1 352 392 1071.
E-mail address: tschmitz@ufl.edu (T.L. Schmitz).

[1] All tests were carried out just after installation of the new machining center in the University of Florida Machine Tool Research Center. Although the machine has five controlled axes (two rotary axes), it was operated as a three-axis prismatic machine for this study.

0141-6359/$ – see front matter © 2007 Elsevier Inc. All rights reserved.
doi:10.1016/j.precisioneng.2007.06.001

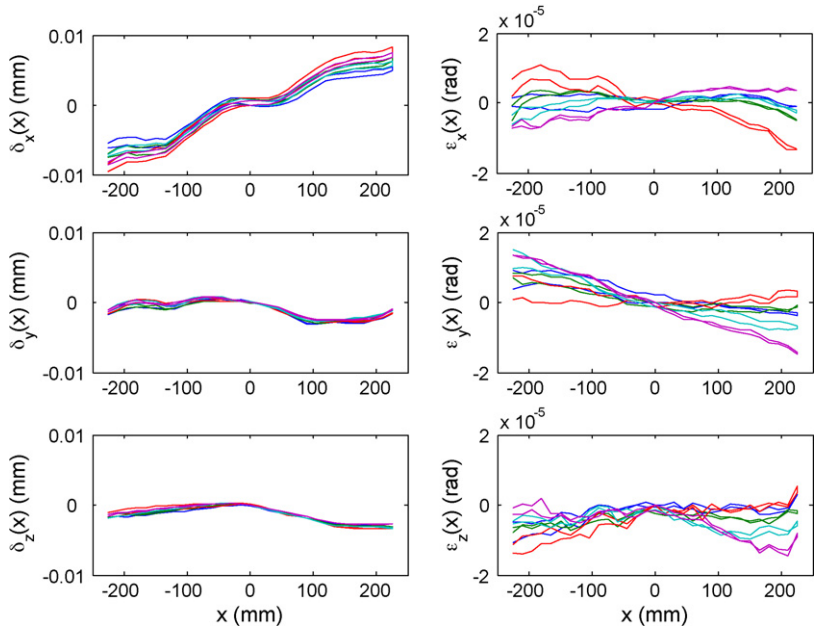

Fig. 1. Error motions for the x-axis. Five repetitions were completed; both the forward and reverse directions are shown.

quasi-static geometric errors and a Monte Carlo simulation for determining the resulting parts errors based on a homogeneous transformation matrix (HTM) formulation are detailed. Next, thermal effects including both spindle thermal growth and variations in the geometric errors with changes in the machine's thermal state are reported. Measurements of the machine's contouring errors at different feed rates are then described. The cutting force error contributions are demonstrated by providing dimensions for parts machined over a range of spindle speeds. Finally, the percent contributions for each source are compared. Note that fixturing errors, tool wear, and quasi-static loading effects (either through self-loading of the machine or part mass) have not been considered and a thermal error index (TEI) [4] evaluation of the machine environment was not completed, although these can be performance limiting factors in some instances.

2. Geometric errors

The parametric errors for the x, y, and z-axes of the machine were measured using the laser ball bar, or LBB [5,6]. The LBB is a two stage telescoping tube (length range from 426 to 896 mm) with a displacement measuring interferometer aligned inside. After an initialization step, the LBB can be used to sequentially measure the six sides of a tetrahedron formed by three sockets attached to the machine table and one socket attached at the tool point. Given the lengths of the six tetrahedron sides, the x, y, z coordinates of the tool point are computed by trilateration. The displacement error motions are determined from the components of the vector difference between commanded and measured tool point coordinates during motions where only a single axis is actuated; the rotations are calculated from the relative error motions of multiple sockets offset from each other on the spindle during the same single axis actuation. Orthogonality errors are determined from best-fit lines to the measured tool point coordinates along each axis of actuation. The LBB was not able to measure the entire machine work volume in a single setup due to limitations in its maximum and minimum lengths (the maximum x, y, and z-axes machine travels were $\{600, 450, \text{and } 450\}$ mm, respectively). However, all subsequent thermal, contouring, and cutting force error measurements were carried out within the LBB measurement volume so the individual effects could be compared. Machining tests were also completed at the same axis locations as the contouring error grid plate measurements.

Table 1
Axis orthogonality errors

Axes	Angle (°)	Δ (arc s)
xy	89.99977	−0.8
yz	89.99934	−2.4
xz	89.99860	−5.1

For this portion of the study, all LBB measurements were completed with the machine in a cold state and were repeated five times. Six degree-of-freedom error motions (three displacements and three rotations) were measured along each axis at 15 mm intervals for both the forward and reverse directions of motion. Fig. 1 shows the five repeated measurement results for each of the six x-axis error motions. Figs. 2 and 3 display the y and z-axes results, respectively. Scatter in the rotational errors is due to the measurement uncertainty of the LBB length (approximately 1 μm) and are likely not reflective of the actual repeatability of the machine[2]. Axis orthogonality data are provided in Table 1, where Δ is the difference from 90°.

[2] The volumetric measurement uncertainty for LBB data was evaluated in [7].

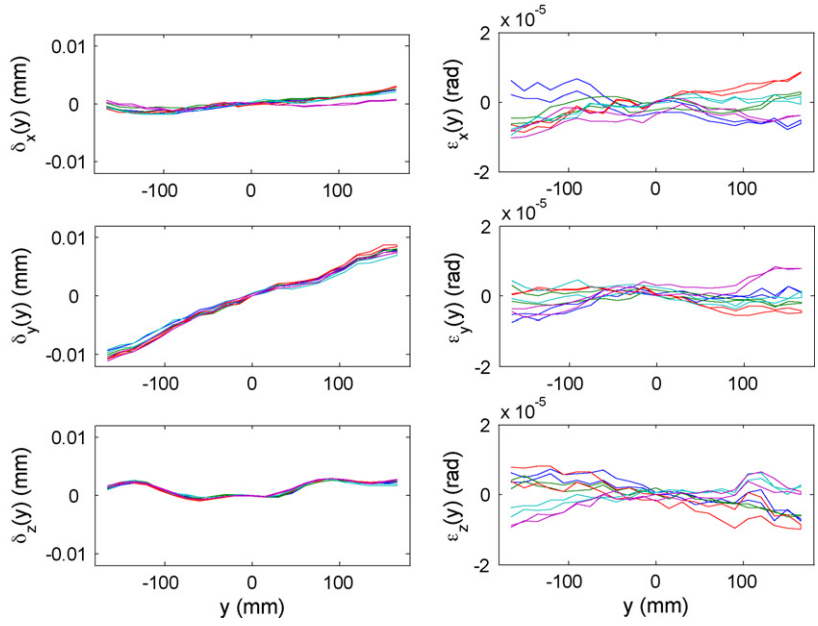

Fig. 2. Error motions for the *y*-axis.

An HTM model of the machine geometry errors was constructed and used to predict the positioning errors at points along the tool path for a circle–diamond–square workpiece. See Fig. 4 for the part geometry and nominal dimensions. The HTM model predicts the actual tool point (center) coordinates, in a coordinate system attached to the workpiece, for any commanded position of the machine axes and any cutting tool geometry. See Eq. (1), where the (4×4) T matrices describe nominal displacements; the (4×4) E matrices are populated by the translational and rotational errors measured by the LBB; and the (4×1) P vectors represent the tool point coordinates in the coordinate system identified in the superscript. See [8]

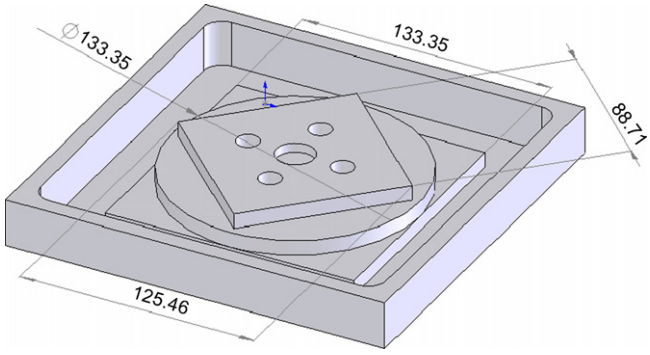

Fig. 4. Circle–diamond–square workpiece dimensions (all values in mm).

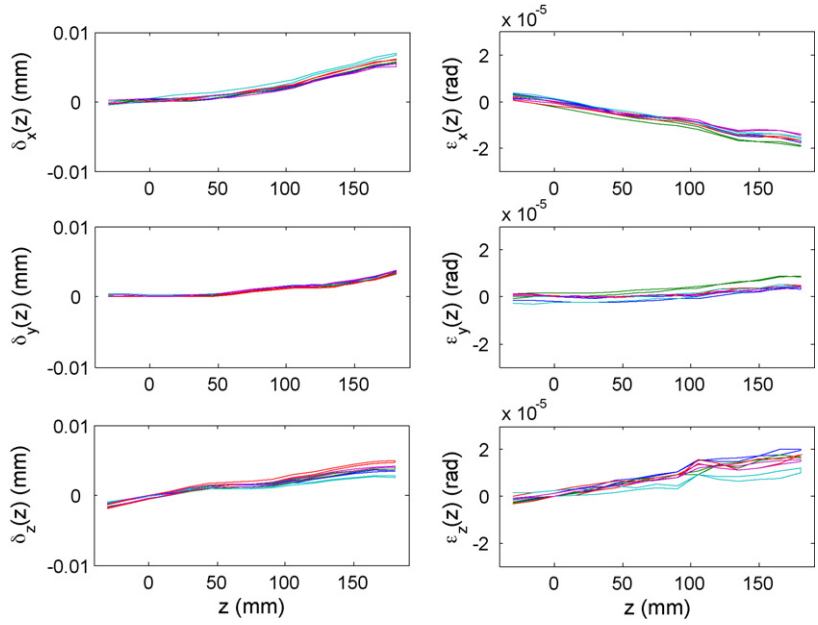

Fig. 3. Error motions for the *z*-axis.

for more information on modeling of machine tool errors using HTMs.

$$^{\text{part}}\vec{P}_{\text{tool}} = {}^{\text{part}}T_x E_x{}^x T_y E_y{}^y T_z E_z{}^z \vec{P}_{\text{tool}} \quad (1)$$

Examples of the T and E matrices for the x-axis are provided in Eq. (2), where x_{command} is the nominal motion in the x direction, the ε terms are the rotation errors, and the δ values are the translation errors. The matrices for the y and z-axes were defined in a similar manner. Note that non-orthogonality between the axes were included as linear terms in the appropriate straightness error functions.

$$^{\text{part}}T_x = \begin{bmatrix} 1 & 0 & 0 & x_{\text{command}} \\ 0 & 1 & 0 & 0 \\ 0 & 0 & 1 & 0 \\ 0 & 0 & 0 & 1 \end{bmatrix}$$

$$E_x = \begin{bmatrix} 1 & \varepsilon_z(x) & -\varepsilon_y(x) & \delta_x(x) \\ -\varepsilon_z(x) & 1 & \varepsilon_x(x) & \delta_y(x) \\ \varepsilon_y(x) & -\varepsilon_x(x) & 1 & \delta_z(x) \\ 0 & 0 & 0 & 1 \end{bmatrix} \quad (2)$$

The measured errors shown in Figs. 1–3 were used in conjunction with the HTM model to predict tool path errors due to machine geometry errors. In order to incorporate the statistical variation in the measurement results, the HTM model was evaluated within a Monte Carlo simulation to determine the resulting spread in machine positioning errors at each commanded point along the tool path. At increments of 2–5 mm along the tool path, a value for each of the 18 (six errors for each of the three machine axes) machine geometric error components was selected from a normal distribution with the mean and standard deviation computed from the five measurement values shown in Figs. 1–3 (at the appropriate axis location). The normal distance from the resulting tool point location to the nominal path was then computed and saved. After many iterations, the spread in error at points along the tool path were computed and the mean value was plotted; see Fig. 5 (a 2000× error magnification has been applied for viewing purposes).

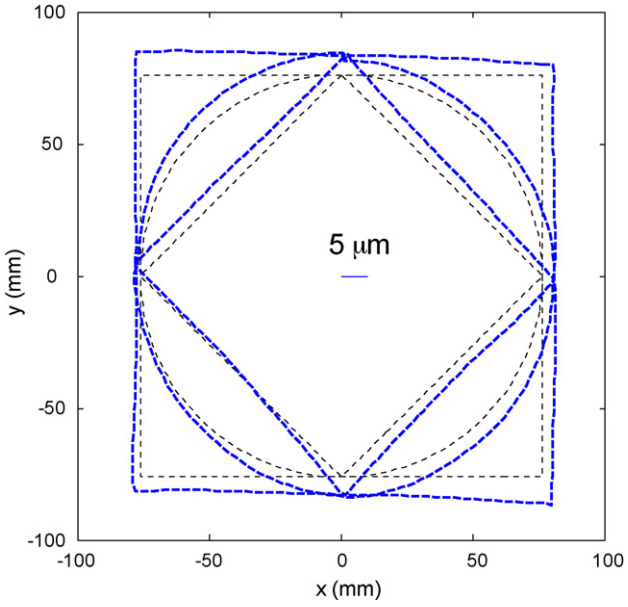

Fig. 5. Predicted tool path errors (heavy dotted line) due to machine geometric errors compared to commanded path (light dashed); the magnification is 2000× (a scale for the error magnification is provided).

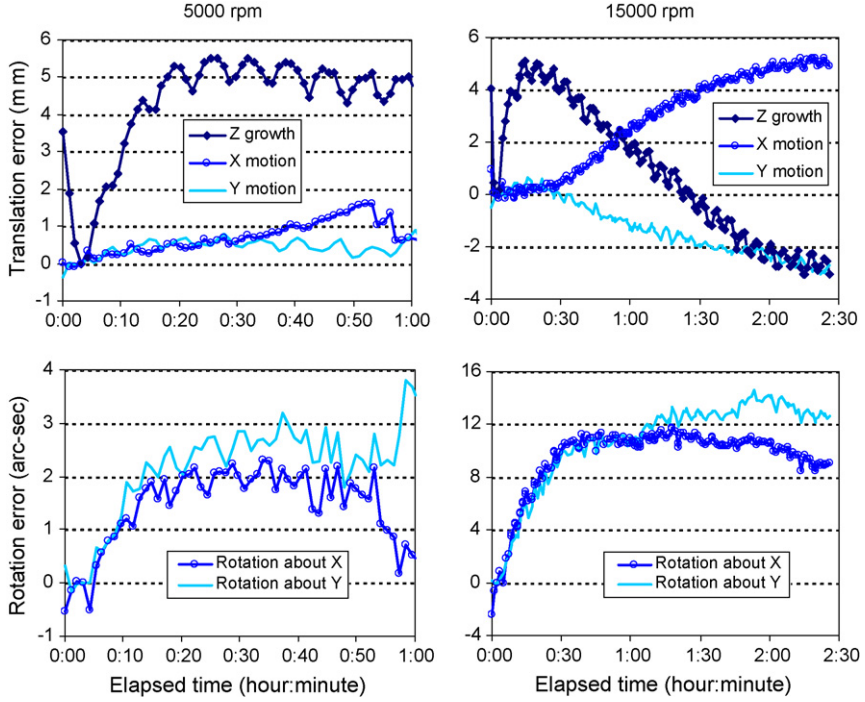

Fig. 6. Spindle thermal growth. The left column provides results for 5000 rpm (top panel is translation errors, the bottom panel is rotation errors); the right column shows results for 15,000 rpm.

3. Thermal errors

Significant heat can be generated during machining [9]; important contributors include the machine axes and spindle motor. Additionally, heat is generated by the shearing action during cutting (much of which is transferred to the deformed chip). Various coolants are often applied to carry away the chips and heat. These heat sources serve to distort the machine geometry and cause errors in machined parts. In this study, the spindle motor and machine axes were considered as primary heat sources, although the heat generated during the cutting process was naturally present during the tests to evaluate cutting force contributions.

Errors associated with spindle thermal growth were measured using a nest of five capacitance sensors reading against a cylindrical carbide tool blank held in the rotating spindle. The capacitance gage outputs were recorded at 1 min intervals as the spindle was exercised from a cold state to (nominally) equilibrium conditions at speeds of 5000 and 15,000 rpm. Results are provided in Fig. 6. The axial (z), lateral (x/y), and tilt (rotations about x and y) errors of the spindle were determined from the capacitance probe data and mean and standard deviations were computed.

To account for thermally induced changes in the geometric errors, LBB measurements were completed at 2 h intervals during a machine warm-up cycle in which the axes were exercised at high speed (no machining). In comparison with the cold-state machine geometric results shown in Figs. 1–3, there was no appreciable change in the trends. The most significant errors were again positioning in the x and y-axes ($\delta_x(x)$ and $\delta_y(y)$, respectively) and the deviations with thermal state were 5 μm or less over an 8 h time period. The Monte Carlo HTM analysis was updated with the new errors, represented by their mean values and standard deviations, from the spindle and warm-up cycle measurements. The new simulation results are provided in Fig. 7.

The thermally induced errors measured for this machine are significantly smaller than thermal errors measured and reported by other researchers for other machines [8,9]. The manufacturer of this machine states that the machine has "thermal error compensation" incorporated into the machine control system, although no technical details are provided on how the compensation is accomplished. There is no provision in the machine software for turning this feature off, so the machine measurements reported here were carried out with this compensation active. While the compensation is not perfect, it does appear to be effective.

4. Contouring errors

CNC motion controllers can introduce tool path trajectory errors, particularly during high-speed motions. Trajectory errors were measured using a Heidenhain grid plate encoder; see Fig. 8. This instrument is capable of dynamic measurement of two-dimensional motions of a read head held in the (non-rotating) machine spindle relative to a grid encoder plate attached to the machine worktable. For these tests, the

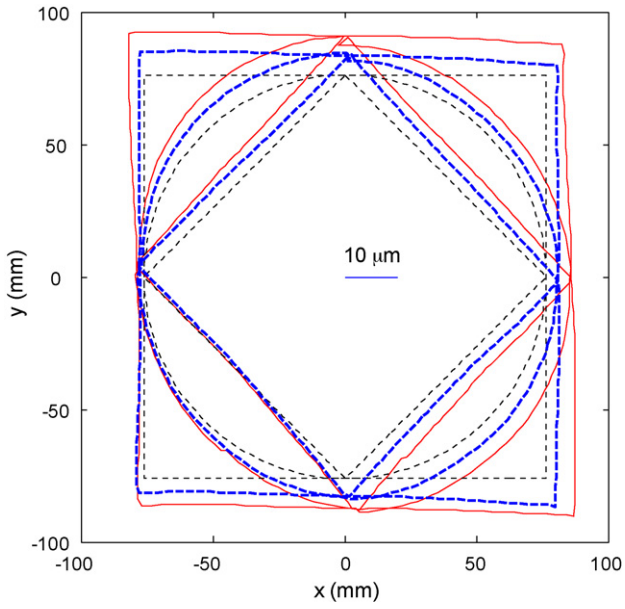

Fig. 7. Predicted tool path errors including thermal effects (2000× magnification).

part program used to machine the test parts was modified to remove z-axis motions associated with the different heights of the circle–diamond–square features. This z-axis motion was assumed to introduce insignificant geometric errors into the tool trajectory, enabling comparison between the tool path recorded by the grid plate encoder and the path predicted by the geometric machine model. Note also that the tool path for a part is defined by the coordinates of the center of the tool. However, since the milling cutter has a finite radius the resulting machined part surface is offset from the tool path. This results in critical part dimensions (circle diameter and diamond/square edge-to-edge distances) that differ from the dimensions of the tool path by the diameter of the cutter. Fig. 9 shows the tool path measured by the grid encoder at two different feed rates, 150 and 8000 mm/min, superimposed on the commanded tool path. The

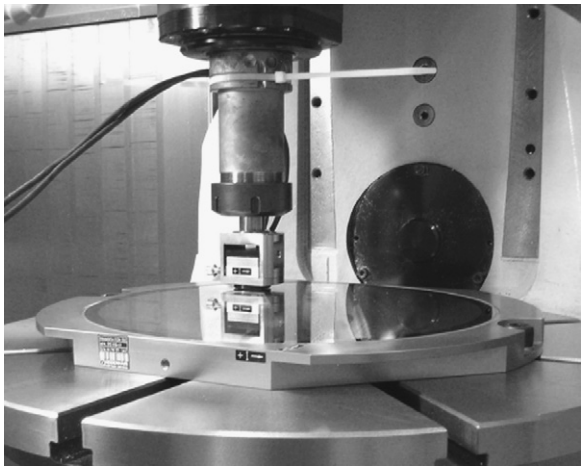

Fig. 8. Grid plate encoder for dynamic, two-dimensional tool trajectory measurements.

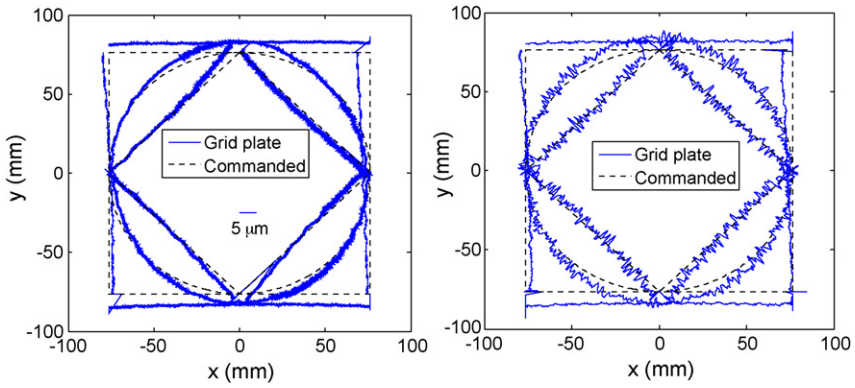

Fig. 9. Tool path measured by grid plate encoder for two feed rates: (left) 150 mm/min and (right) 8000 mm/min.

difference between the commanded and measured paths is again magnified by a factor of 2000 for viewing purposes.

If the geometric error simulation results shown in Fig. 5 are compared with the grid encoder measurements shown in Fig. 9, significant similarities are observed. Additionally, it is seen that the path errors do not change appreciably with feed rate for this machine (although the high spatial frequency noise does increase). These results suggest that the dynamic contouring errors are negligible in comparison to the geometric errors on this CNC machine.

5. Cutting force errors

Errors introduced by the cutting process dynamics take the form of surface location errors, or SLE [10–18]. Milling is, by definition, an interrupted cutting process in which the teeth on the cutting tool repeatedly impact the part and cut away small chips from the workpiece. Therefore, even under stable (or chatter-free) cutting conditions, the tool experiences periodic forced vibrations. The magnitude and phase of these vibrations depend on the process parameters, such as the dynamic response of the system (represented by the frequency response function, or FRF), the excitation frequency (which depends on the spindle speed and the number of teeth on the cutter), the force model represented by the cutting coefficients (of the tool/workpiece system) which relate the cutting force to the undeformed chip area, the radial and axial depths of cut, the feed per tooth, and the cutter helix angle. The location of the machined part surface is determined by the location of each tooth on the vibrating tool at the instant it enters (up milling) or exits (down milling) the cut. Depending on the excitation frequency (determined by the spindle speed and number of cutter teeth) and its relationship to the system natural frequencies, the tool may lie on either side of (or on) the commanded path at this instant and, thus, may remove less material than commanded (undercutting) or more material than commanded (overcutting). Fig. 10 shows an example of undercutting.

An interesting characteristic of stable milling operations is that, because the tool experiences forced vibration at the tooth passing frequency, the vibrational response occurs at the same frequency and the amplitude and phase of the vibration is approximately constant relative to the excitation. This results in the generation of a smooth machined surface even though the tool is undergoing vibrational excursions perpendicular to that surface. In high-speed milling, cutting speeds are normally chosen to place the tooth passing frequency near the system natural frequency to help stabilize against chatter. In this situation, the vibrational amplitude of the tool can be large and, due to the lowly damped nature of the system in general, the phase between force and displacement can vary significantly with small changes in spindle speed. This leads to potentially large amplitude SLE (undercut or overcut).

As described in Section 4, the grid plate was used to measure the geometric and controller effects only. Naturally, the SLE effects were excluded since cutting did not take place. For the machined part SLE tests, the geometric and contouring errors were again present since the tool follows the same spatial path under machine control as in the grid plate tests, but the effect of forced vibrations on the final part dimensions was included as well. The tool path was defined such that the tool center followed the same contour used in the grid plate tests (with feature critical dimensions of 152.4 mm). However, as noted previously, when placing the cutting tool center along this tool path, the critical feature dimension changed due to the cutter radius. The resulting diamond was slightly smaller than the circle and square; the diamond's nominal critical dimension was 125.46 mm (across the diamond faces) while the circle diameter and square side length was nominally 133.35 mm. See Fig. 4, where the circular pocket and four surrounding holes were machined prior to the circle–diamond–square features in order to provide reference features to define the part coordinate system and to facilitate fixturing.

The cutting tests were performed with a 19.05 mm diameter, four flute helical endmill clamped in a collet-type holder with a 57 mm overhang (20,000 rpm, 16 kW HSK-63A spindle). The

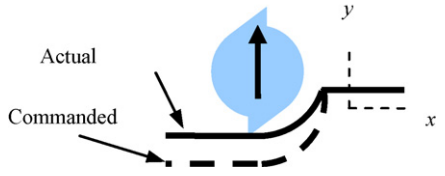

Fig. 10. Undercut surface in down milling due to the cutter vibration state at cut exit. The error is dominated by y direction vibrations.

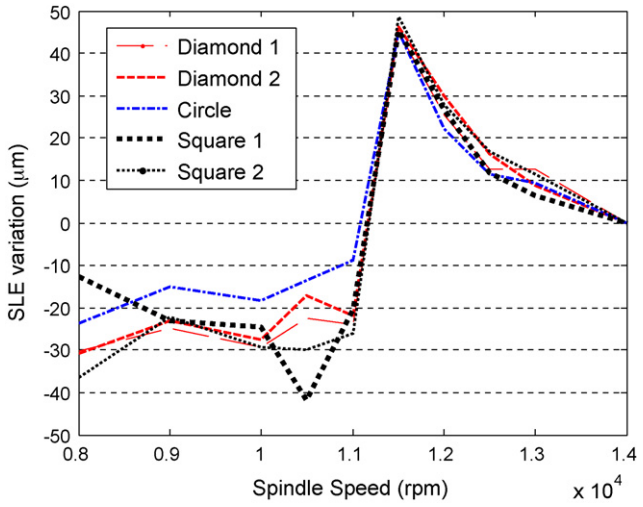

Fig. 11. SLE results for circle, diamond, and square. The data are normalized to the top spindle speed of 14,000 rpm. For all features the SLE is strongly dependent on spindle speed.

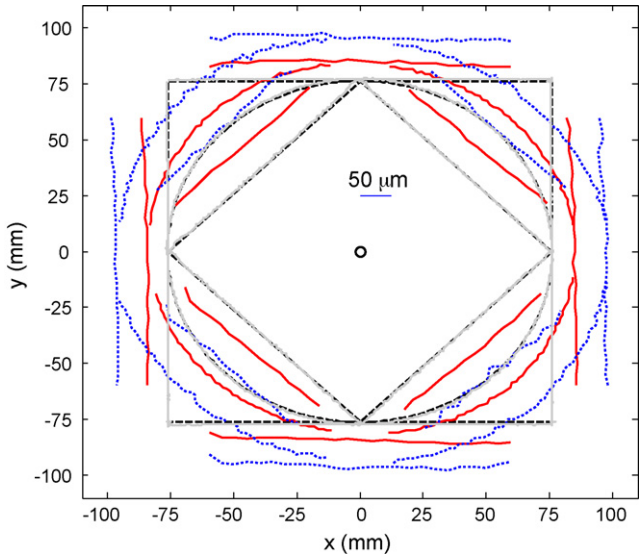

Fig. 12. Comparison of tool path (grey solid line), nominal path (dashed) and actual part errors for two spindle speeds—11,500 rpm (dotted) and 14,000 rpm (solid). The error magnification is 250×.

parts were first rough machined while leaving enough material to perform finishing cuts at 25% radial immersion (i.e., 25% of the cutter diameter) and 8 mm axial depth of cut (the height of the circle, diamond, and square features). All of the test cuts were performed with a feed per tooth of 0.15 mm/tooth. The spindle speeds were: {8000, 9000, 10,000, 10,500, 11,000, 11,500, 12,000, 12,500, 13,000, and 14,000} rpm. The 10 parts were then measured on a touch trigger probe coordinate measuring machine (CMM)[3].

In the case of the diamond and square, the side lengths where determined by measuring the distances between opposing sides. The circle was divided into four arcs and each was measured individually. The arc lengths were selected to avoid the diamond vertices. They were then fit to a single circle; the circle measurements correspond to this fit performed by the CMM software. To compute SLE from these data, the actual dimensions for these features were differenced with the commanded dimensions (10 total parts corresponding to the 10 different spindle speeds). The dimensional errors were then divided by two (i.e., a constant SLE was assumed to be present on all machined surfaces so the total feature dimensional error is twice the SLE for each surface). Additionally, the errors for the three features were normalized to zero at the top spindle speed (14,000 rpm) for presentation purposes. Although the absolute magnitudes of SLE for the circle, diamond, and square features differed slightly, this normalization clarified the similarities in the SLE trends with spindle speed for each feature. See Fig. 11, where the two curves for the diamond and square correspond to the measurements across the two available faces for each. As expected, the same trends are observed in all cases.

The largest change in SLE occurs near 11,000 rpm, where the tooth passing frequency (i.e., the spindle speed multiplied by the number of teeth) coincides with the tool's fundamental bending natural frequency. It is of interest to note that this spindle speed also corresponds to the peak of the stability lobe which identifies a region of increased allowable axial depth of cut without chatter; the well-known stability lobe diagram is often used to select preferred spindle speeds in high-speed machining applications [19]. The total range of SLE variation is approximately 70 μm, which is significantly larger than the errors measured by the LBB and grid plate. These results suggest that the process dynamics should be considered in addition to the part geometry in evaluating machine tool performance by a machined test part (such as the NAS 979 [3]). The reader may note that spindle speed was the only process parameter varied during the SLE tests. Varying the axial depth, radial depth, and feed per tooth, for example, would increase or decrease the SLE (a proportional relationship is generally assumed), but maintain the same general profile of the SLE versus spindle speed curve. See, for example, Refs. [16,18] for a more detailed description and modeling approaches.

To make a direct comparison with the dynamic tool path errors shown in Fig. 9, the 8000 mm/min path from the grid encoder is plotted together with the part dimensions determined from the CMM measurements for spindle speeds of 11,500 and 14,000 rpm. See Fig. 12, where the error magnification is now 250× (note that this figure shows part dimensions relative to the commanded feature size—no normalization was applied as in Fig. 11). It is seen that the tool path errors are barely distinguishable in comparison to the SLE contributions.

6. Error comparison

A summary of the percent contribution of each error source to workpiece accuracy for this machine tool (and selected toolholder combination) is provided in Fig. 13 using the worst-case errors for all sources. The maximum contribution of geometric error to part inaccuracy was calculated to be 6 μm (root sum square of errors in each coordinate direction). Thermal growth

[3] The CMM accuracy is estimated as 5 μm or better over the workpiece measurement volume.

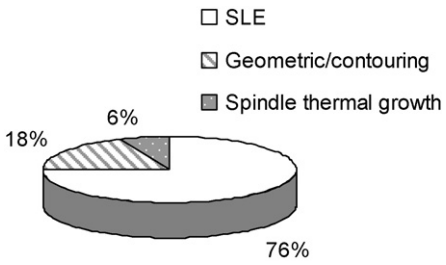

Fig. 13. Percent contribution of error sources to workpiece accuracy.

of the machine contributed an additional 6 μm (worst case) to the cold-state geometric error effects. The combined geometric and controller error sources obtained from the grid plate measurements gave a maximum deviation from the commanded path of 11 μm at the 8000 mm/min feed rate. At 150 mm/min, the maximum deviation reduced to 6 μm, which can be attributed to geometric error sources. The machine effectively compensated for spindle thermal growth, limiting the z-axial growth to 5 μm as shown in Fig. 6. The range of the SLE test data was approximately 70 μm although this varies with the tool-holder-spindle FRF, workpiece material, and selected spindle speed. At the worst spindle speed selection, 11,500 rpm, the features were larger than commanded by approximately 45 μm, while at a slightly different speed, 10,500 rpm, the features averaged approximately 25 μm smaller than the commanded size. At some speed between these, it should be possible to reduce the SLE to near zero. For this small range of spindle speeds, any of which would be reasonable and valid choices for high-speed milling applications, the SLE contribution to part error can be significantly larger than the other sources, but can also be reduced to near zero if the correct speed is selected. However, current procedures for selecting spindle speed in high-speed milling are primarily oriented toward chatter avoidance and provide less guidance for reducing part dimensional errors.

7. Conclusions

In this paper, a case study that quantified the relative contributions of geometric, thermal, contouring, and cutting force errors to part errors for a circle–diamond–square workpiece geometry under selected cutting conditions typical of high-speed milling is described. The quasi-static geometric errors for a representative high-speed machining center were measured using the laser ball bar. Thermal effects were identified by repeating these measurements at regular intervals during a warm-up period. Spindle thermal growth errors were measured using a capacitance gage nest. These results were incorporated into a Monte Carlo simulation to predict the resulting part errors using a homogeneous transformation matrix formulation. Contouring errors were recorded at different feed rates using a grid plate encoder. The cutting force error contributions were identified by machining the selected part geometry over a range of spindle speeds and measuring the resulting feature dimensions. A comparison of these error sources showed that the cutting force error can be an order of magnitude larger than the combined effect of the other error sources for some choices of spindle speeds, but may become insignificant at slightly different spindle speeds.

Acknowledgements

The authors gratefully acknowledge partial support for this study from BWXT Y-12, Oak Ridge, TN and helpful suggestions from W. Barkman and P. Jacobs, BWXT Y-12.

References

[1] Schlesinger G, Koenigsberger. Testing machine tools: for the use of machine tool makers, users, inspectors and plant engineers. New York, NY: Pergamon Press; 1978 [originally published in 1927 as Inspection Tests on Machine Tools].
[2] Hocken R, editor. Technology of machine tools, machine tool accuracy, UCRL-52960-5, vol. 5. Livermore, CA: Lawrence Livermore National Laboratory; 1980.
[3] National Aerospace Standards, 1969, NAS 979, Uniform Cutting Tests, NAS 900 Series metal cutting equipment specifications.
[4] American Society of Mechanical Engineers. ASME B5. 54-1992 Methods for performance evaluation of computer numerically controlled machining centers. New York, NY: American Society of Mechanical Engineers; 1993.
[5] Ziegert JC, Mize CD. The laser ball bar: a new instrument for machine tool metrology. Precision Eng 1994;16(4):259–67.
[6] Srinivasa N, Ziegert JC, Mize CD. Spindle thermal drift measurement using the laser ball bar. Precision Eng 1996;18(2):118–28.
[7] Canning S, Ziegert J, Schmitz T. Uncertainty of spatial coordinate measurements using trilateration. Trans NAMRI/SME 2005;33:121–8.
[8] Slocum A. Precision machine design. Englewood Cliffs, NJ: Prentice-Hall, Inc.; 1992.
[9] Bryan J. International status of thermal error research. Ann CIRP 1990;39(2).
[10] Kline W, DeVor R, Shareef I. The prediction of surface accuracy in end milling. J Eng Ind 1982;104:272–8.
[11] Kline W, DeVor R, Lindbeg J. The prediction of cutting forces in end milling with application to cornering cuts. Int J Mach Tool Des Res 1982;22:7–22.
[12] Tlusty J. Effect of end milling deflections on accuracy. In: King RI, editor. Handbook of high-speed machining technology. NY: Chapman and Hall; 1985. p. 140–53.
[13] Sutherland J, DeVor R. An improved method for cutting force and surface error prediction in flexible end milling systems. J Eng Ind 1986;108:269–79.
[14] Montgomery D, Altintas Y. Mechanism of cutting force and surface generation in dynamic milling. J Eng Ind 1991;113(2):160–8.
[15] Altintas Y, Montgomery D, Budak E. Dynamic peripheral milling of flexible structures. J Eng Ind 1992;114(2):137–45.
[16] Schmitz T, Ziegert J. Examination of surface location error due to phasing of cutter vibrations. Precision Eng 1999;23(1):51–62.
[17] Mann BP, Bayly PV, Davies MA, Halley JE. Limit cycles, bifurcations, and accuracy of the milling process. J Sound Vibration 2004;277:31–48.
[18] Schmitz T, Mann B. Closed form solutions for surface location error in milling. Int J Mach Tools Manuf 2006;46:1369–77.
[19] Smith S, Tlusty J. An overview of modeling and simulation of the milling process. J Eng Ind 1991;113:169–75.